Molecular Ordering in Monolayers of an Alkyl-Substituted Perylene-Bisimide Dye by Attenuated Total Reflectance Ultraviolet–Visible Spectroscopy

WALTER J. DOHERTY III,* ADAM G. SIMMONDS, SERGIO B. MENDES, NEAL R. ARMSTRONG,† and S. SCOTT SAAVEDRA†

Department of Chemistry (W.J.D., A.G.S., S.B.M., N.R.A., S.S.S.), and Optical Sciences Center (S.B.M., N.R.A.), University of Arizona, Tucson, Arizona 85721

Surface-relative orientational parameters were determined for monolayer films of N, N′-ditridecylperylenetetracarboxylic dianhydridediimide (C_{13}-PTCDI) in terms of the relative electronic transition dipole strengths, providing a three-dimensional view of the absorption dipole distribution. In order to obtain a macroscopically ordered film, C_{13}-PTCDI was deposited by (1) horizontal Langmuir–Blodgett (LB) transfer onto methyl- and phenyl-silanized glass, and (2) vapor deposition onto oriented films of poly(tetrafluoroethylene) (PTFE) on glass. Films of LB-deposited C_{13}-PTCDI were found to be completely isotropic prior to annealing. After annealing, these films remained isotropic in the plane of the substrate while the out-of-plane anisotropy was significantly enhanced. In contrast, films of C_{13}-PTCDI vapor deposited onto oriented poly(tetrafluoroethylene) (PTFE)-modified substrates yielded films with a high degree of both in- and out-of-plane anisotropy. Atomic force microscopy (AFM) images of both the LB- and vapor-deposited films show substantial differences in film morphology and long-range order. These results demonstrate that molecular orientation in C_{13}-PTCDI films can be controlled by varying substrate surface chemistry and post-deposition processing.

Index Headings: **Attenuated total reflection; ATR; Molecular orientation; Perylene.**

INTRODUCTION

The development of organic electronics depends largely on the ability to control the charge transport characteristics of the organic material. For the majority of molecular semiconductors, these characteristics exhibit a dependency on the degree of overlap of molecular orbitals in adjacent molecules.[1–3] This, in turn, displays a strong dependency on the degree of ordering and the relative orientation of the molecules.[4] The exciton diffusion length in an organic photovoltaic solar cell, for example, increases substantially with increased ordering of the organic layer, resulting in a higher energy conversion efficiency.[5–10] In addition, many materials, such as ordered films of phthalocyanines,[11,12] have shown significant conductivity anisotropy depending on the orientation of the molecule relative to the desired direction of charge flow.

Perylene derivatives, especially N,N′-dialkyl-3,4,9,10-perylenetetracarboxyldiimides (PTCDI), have been studied as possible organic layers in photovoltaic cells, due to the ease with which these molecules assemble into liquid crystalline arrays upon vapor deposition[5,13,14] or compression on a Langmuir–Blodgett (LB) trough.[8,15–17] Several studies[3,13] have shown that strong π–π interactions between the perylene cores result in a ''slipped stack'' cofacial arrangement of the molecules in which the planes of the perylene cores of adjacent molecules in a stack are parallel with a slight lateral offset.

The molecular orientation of substrate-supported PTCDI materials has been investigated with variable results depending on the choice of substituents, deposition technique, surface composition, and analytical technique. In evaporated films of alkyl-substituted PTCDI derivatives, the angle between the perylene core and the π–π stacking axis of the aggregates has been determined to be 64° based on X-ray diffraction studies and molecular geometry.[13] Aroca and co-workers[15–17] have studied molecular orientation in LB films of a series of perylene derivatives substituted asymmetrically with alkyl chains of varying length. The absorbance anisotropy of characteristic vibrational transition dipoles (C=C and C=O stretches) was measured using reflection–absorption infrared spectroscopy (RAIRS) and transmission infrared spectroscopy. These experiments yielded ensemble-averaged tilt angles, relative to the substrate normal, of 40° and 66° for the long and short axes of the molecule, respectively.

Gregg and co-workers used molecular modeling, in combination with X-ray diffraction measurements and pressure-area isotherms obtained by LB compression, to examine a series of polyethylene glycol substituted PTCDI derivatives deposited on glass substrates.[8,9] In these films, the molecules preferentially orient in an ''edge-on'' fashion, with an angle of 32° or less between the surface normal and the long axis of the molecular dipole. The angle between the long axis of the perylene core and the π–π stacking axis of the aggregated structure was 47°.[8]

In all of the studies cited above, determining molecular orientation in a substrate-supported film required making assumptions with respect to molecular geometry, packing dynamics, and/or substrate effects. For example, to calculate tilt angles in LB films of perylene derivatives, Aroca and co-workers made three major assumptions: (1) The orientation distribution was assumed to be infinitely narrow (i.e., a delta function). (2) The relative orientation of the vibrational transition dipoles with respect to the molecular geometry was assumed. (3) The molecular orientation of the PTCDI core was assumed to be identical on both the silver-coated RAIRS substrates and the trans-

Received 23 May 2005; accepted 2 August 2005.

* Current address: Department of Physics and Measurement Technology (IFM), Linköping University, SE-581 83 Linköping, Sweden.

† Authors to whom correspondence should be sent.

0003-7028/05/5910-1248$2.00/0

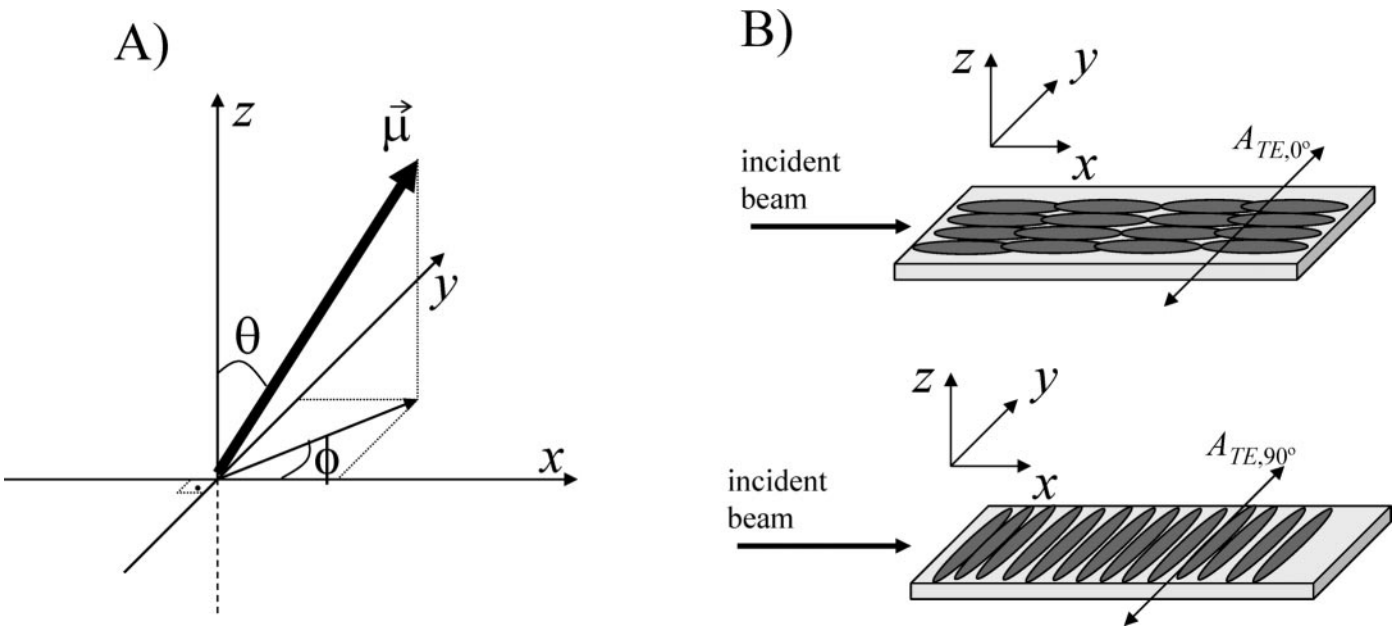

FIG. 1. (**A**) The *x*–*y* plane represents the surface of the IRE, with the *z*-axis as the surface normal. The electronic transition vector is represented as $\vec{\mu}$, and θ is the angle between $\vec{\mu}$ and the *z*-axis. The angle between the *x*-axis and the projection of $\vec{\mu}$ onto the *x*–*y* plane is ϕ. (**B**) Top: Light propagates, via internal reflection in the *x*–*z* plane, in a microscope slide coated with a C_{13}-PTCDI film. The absorbance of TE polarized light is denoted $A_{TE,0°}$. Bottom: By rotating the slide 90° relative to the incident beam or by changing the conditions under which the C_{13}-PTCDI film is deposited, the absorbance for TE polarized light, now denoted $A_{TE,90°}$, probes the other in-plane transition dipole component.

mission infrared (IR) substrates (Ge or ZnS), which allowed the data from the two experiments to be combined.

Direct measurement of the strength of the electronic transition vector components, without relying on such assumptions, offers the advantages of experimental simplicity and accuracy. Here we demonstrate the use of broadband attenuated total reflectance (ATR) spectroscopy[18] to measure both in-plane and out-of-plane orientational parameters of monolayer films of a ditridecyl-substituted PTCDI derivative without invoking *a priori* models or making assumptions about substrate–film interactions or the orientation distribution. Orientational parameters were measured on LB-deposited films of C_{13}-PTCDI before and after annealing, and on films formed by vapor deposition on oriented poly(tetrafluoroethylene) (PTFE) substrates. These studies parallel research we have recently reported using similar approaches to determine the orientation of discotic mesophase materials (phthalocyanines), as monolayer and bilayer supported thin films, using ATR spectroscopies without assumptions for orientation distribution.[19]

THEORY

In Fig. 1A, the orientation of a linear electronic transition dipole vector, $\vec{\mu}$, relative to the surface of an internal reflection element (IRE) is defined by two angles, θ and ϕ, that describe the position of $\vec{\mu}$ with respect to the axes of the laboratory coordinate system. The internally reflected probe beam propagates in the *x*–*z* plane, and the *x*–*y* plane corresponds to the interface between the molecular film and the IRE surface.

The absorbance of the film is described by the general expression[20]

$$A = \langle(\vec{\mu}\cdot\vec{E})^2\rangle \tag{1}$$

where $\vec{E}$ is the electric field vector of the optical beam and the angle brackets represent the ensemble average of the individual molecular dipole orientations. For light polarized perpendicular (transverse electric (TE)) and parallel (transverse magnetic (TM)) to the plane of incidence, Eq. 1 becomes

$$A_{TE} = \langle(\mu_y E_y)^2\rangle = \langle\mu_y^2\rangle E_y^2 \tag{2a}$$

$$A_{TM} = \langle(\mu_x E_x + \mu_z E_z)^2\rangle = \langle\mu_x^2\rangle E_x^2 + \langle\mu_z^2\rangle E_z^2 \tag{2b}$$

where E_i and μ_i are the magnitudes of the electric fields and the transition dipole components along the three laboratory axes ($i = x, y, z$). Since the orientation distribution of the sample should be symmetric about the *y*–*z* plane (see below and Experimental section), then $\langle\mu_x\mu_z = 0$. The sum of the ensemble average values of the squared transition dipole components is related to the total dipole strength, μ, by:

$$\langle\mu_x^2\rangle + \langle\mu_y^2\rangle + \langle\mu_z^2\rangle = \mu^2 \tag{3}$$

The degree of in-plane (azimuthal) anisotropy in the molecular film can be determined by measuring the absorbance of a probe beam in two orthogonal sample orientations, here called 0°- and 90°-orientation, and shown schematically in Fig. 1B for TE polarization. Experimentally, the deposition conditions were controlled to produce sample films whose symmetry axes were orthogonal to each other (see Experimental section). By applying Eq. 2 for the two sample orientations, the absorbance of a molecular film can be expressed by:

$$A_{TE,0°} = \langle\mu_y^2\rangle E_y^2 \tag{4a}$$

$$A_{TE,90°} = \langle\mu_x^2\rangle E_y^2 \tag{4b}$$

for TE polarization, and

$$A_{TM,0^\circ} = \langle \mu_x^2 \rangle E_x^2 + \langle \mu_z^2 \rangle E_z^2 \quad (5a)$$

$$A_{TM,90^\circ} = \langle \mu_y^2 \rangle E_x^2 + \langle \mu_z^2 \rangle E_z^2 \quad (5b)$$

for TM polarization. The absorbance dichroism for each polarization is defined by

$$r_{TE} \equiv \frac{A_{TE,0^\circ}}{A_{TE,90^\circ}} = \frac{\langle \mu_y^2 \rangle}{\langle \mu_x^2 \rangle} \quad \text{and} \quad (6)$$

$$r_{TM} \equiv \frac{A_{TM,0^\circ}}{A_{TM,90^\circ}} = \frac{\langle \mu_x^2 \rangle E_x^2 + \langle \mu_z^2 \rangle E_z^2}{\langle \mu_y^2 \rangle E_x^2 + \langle \mu_z^2 \rangle E_z^2} \quad (7)$$

Combining Eqs. 3, 6, and 7 yields the following expressions, which describe the squared magnitudes of the transition dipole components along the three coordinate axes, and depend only on the electric field amplitudes (E_x and E_z) and the experimentally determinable parameters r_{TE} and r_{TM}:

$$\frac{\langle \mu_x^2 \rangle}{\mu^2} = \frac{E_z^2(1 - r_{TM})}{E_z^2(1 + r_{TE} - r_{TM} - r_{TE}r_{TM}) + E_x^2(-1 + r_{TE}r_{TM})} \quad (8a)$$

$$\frac{\langle \mu_y^2 \rangle}{\mu^2} = \frac{E_z^2(1 - r_{TM})r_{TE}}{E_z^2(1 + r_{TE} - r_{TM} - r_{TE}r_{TM}) + E_x^2(-1 + r_{TE}r_{TM})} \quad (8b)$$

$$\frac{\langle \mu_z^2 \rangle}{\mu^2} = \frac{E_x^2(-1 + r_{TE}r_{TM})}{E_z^2(1 + r_{TE} - r_{TM} - r_{TE}r_{TM}) + E_x^2(-1 + r_{TE}r_{TM})} \quad (8c)$$

The orientation angles ϕ and θ shown in Fig. 1 can be related to the expressions in Eq. 8 through a pair of rotation matrices describing the angular dependencies of $\langle \mu_x^2 \rangle$, $\langle \mu_y^2 \rangle$, and $\langle \mu_z^2 \rangle$ shown below,[21]

$$\begin{pmatrix} \mu_x \\ \mu_y \\ \mu_z \end{pmatrix} = \begin{pmatrix} \cos\phi & -\sin\phi & 0 \\ \sin\phi & \cos\phi & 0 \\ 0 & 0 & 1 \end{pmatrix} \begin{pmatrix} \cos\theta & 0 & \sin\theta \\ 0 & 1 & 0 \\ -\sin\theta & 0 & \cos\theta \end{pmatrix} \begin{pmatrix} 0 \\ 0 \\ \mu \end{pmatrix}$$

$$= \begin{pmatrix} \cos\phi \sin\theta \\ \sin\phi \sin\theta \\ \cos\theta \end{pmatrix} \mu \quad (9)$$

from which the following relations can be derived[19]

$$\frac{\langle \mu_x^2 \rangle}{\mu^2} = \langle \cos^2\phi \sin^2\theta \rangle \quad (10a)$$

$$\frac{\langle \mu_y^2 \rangle}{\mu^2} = \langle \sin^2\phi \sin^2\theta \rangle \quad (10b)$$

$$\frac{\langle \mu_z^2 \rangle}{\mu^2} = \langle \cos^2\theta \rangle \quad (10c)$$

Thus the orientation parameters of the linear electronic transition vector shown in Fig. 1A can be experimentally determined by application of Eqs. 8 and 10.

EXPERIMENTAL

Langmuir–Blodgett Film Preparation. Substrates were glass microscope slides (thickness ≈ 1 mm, Gold Seal Products, #3010) or silicon wafers (Wacker, [1,1,1]). Prior to film deposition, glass substrates were subjected to initial cleaning by light mechanical scrubbing with Alconox cleaner using a cotton pad and rinsed with deionized water (Barnstead Nanopure, 18.2 MΩ·cm). Initial cleaning of silicon substrates consisted of immersion in fresh Piranha solution (30:70 v/v H_2O_2: conc. H_2SO_4) for 15 min, followed by rinsing in deionized water. This treatment produces an oxide layer thickness of approximately 20 Å.[22] Immediately following initial cleaning, all substrates were blown dry with nitrogen and placed in air plasma (Harrick PDC-3XG) for 15 min at 25 W. Immediately thereafter, substrates were rendered hydrophobic, to enhance the transfer efficiency of the LB films, by sonication in a mixture of 1,1,1,3,3,3-hexamethyldisilazane (HMDS) and 1,3-diphenyl-1,1,3,3-tetramethyldisilazane (DPTMDS) dissolved in chloroform (5:5:90 v/v HMDS:DPTMDS:$CHCl_3$) for 30 min.[23,24] Silanized substrates were stored in air in a sealed vessel and cleaned immediately before LB film deposition by sonication in chloroform for a minimum of 30 min.

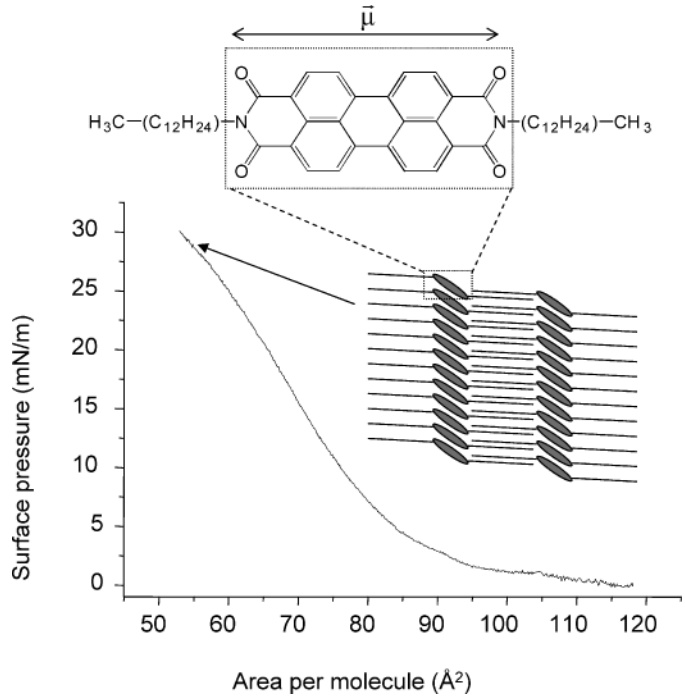

FIG. 2. The electronic absorption transition moment, $\vec{\mu}$, is parallel to the long molecular axis of C_{13}-PTCDI.[21] The pressure-area isotherm of a Langmuir film of C_{13}-PTCDI is shown, along with the proposed packing geometry (top view) of the molecules when compressed to 55 Å² per molecule.[8,13,14]

Monolayer films of N,N′-ditridecyl-3,4,9,10-perylenetetracarboxylicdiimide (C_{13}-PTCDI) (Aldrich, 97%) were prepared on a Nima model 611D LB trough using 10% trifluoroacetic acid in dichloromethane as the spreading solvent.[17] The C_{13}-PTCDI solution (0.11 mM, 750 μL) was spread onto a deionized water subphase at room temperature. The film was left on the trough for approximately 45 min prior to compression to allow complete evaporation of spreading solvent and film equilibration. Compression was performed at a rate of 45 mm/s until a condensed-phase monolayer was observed, as evidenced by the first phase transition ''shoulder'' in the pressure-area isotherm,[11] corresponding to approximately 50–55 Å²/molecule (Fig. 2).

Monolayer LB films were deposited onto silanized

substrates using a horizontal transfer[18,23,24] in which the substrate plane was parallel to the trough surface. One-half of each substrate was covered lengthwise with another silanized glass slide immediately before film deposition, as described elsewhere.[18,25] This prevented deposition on the covered half of the substrate, which was subsequently used as a spectroscopic blank. The liquid crystalline behavior of the film prevented determination of an accurate transfer ratio, as molecules remaining at the air–water interface did not spontaneously redistribute. Visual inspection of the substrate after deposition revealed a homogeneous film, suggesting quantitative or near-quantitative transfer. After deposition, films were removed from the subphase and blown dry with nitrogen. Unannealed films were analyzed immediately. Annealed films were held at 100 °C for three hours in air and returned to room temperature prior to analysis.

Langmuir–Blodgett film-coated substrates were prepared in pairs. For each Langmuir film, horizontal deposition was performed simultaneously on two substrates with orthogonal orientations, one with its long axis parallel (denoted 0°-orientation) and the other perpendicular (denoted 90°-orientation) to the compression barriers of the Langmuir trough (see Fig. 1B). This procedure produced pairs of substrates with azimuthally orthogonal orientations, allowing ATR spectroscopy to be performed with the beam propagating either parallel or perpendicular to the direction of compression.

PTFE-Modified Substrates and Vapor Deposition of C_{13}-PTCDI. Substrates were microscope slides cleaned as described above. Oriented films of poly(tetrafluoroethylene) (PTFE) were deposited mechanically according to the procedure described by Wittmann and Smith,[26] briefly described here. A clean slide was heated to 130 °C on a hotplate. A 1 cm × 1 cm block of Teflon, attached to a 1-kg weight, was pulled across the surface of the substrate at a constant rate of approximately 1 mm/s. Pairs of substrates with azimuthally orthogonal PTFE films were prepared by pulling the Teflon block along either the short or the long axis of the glass slide. Sessile water contact angles were measured on bare glass and PTFE-modified glass using a 3 μL drop volume on a Krüss Drop Shape Analysis System. Ellipsometric thickness of the PTFE film was measured at 590 nm at incident angles of 60° and 70° on a variable angle of incidence spectroscopic ellipsometer (VASE, J. A. Woollam Company), assuming a refractive index of 1.31.[27]

C_{13}-PTCDI was purified once by zone sublimation. The matrix-assisted laser desorption ionization (MALDI) mass spectrum (not shown) of purified C_{13}-PTCDI was dominated by the protonated molecular ion at *m/z* 755.5, indicating that the tridecyl derivative resists thermal breakdown during evaporation under vacuum. Attempts to deposit LB monolayers of C_{13}-PTCDI onto PTFE-modified substrates resulted in non-adherent, inhomogeneous films. Instead, films were vapor deposited onto the PTFE-modified substrates from a crucible source held at 370 °C at 4×10^{-6} torr. The substrate temperature was held at approximately 100 °C. The deposition was performed for 1 min at a rate of 0.5 Å/s (total mass thickness 3 nm), measured using a quartz crystal microbalance. This amount of material approximates the deposition of one equivalent monolayer based on the molecular geometry shown in Fig. 2. After deposition, substrates were allowed to cool to room temperature over 1.5–2 h before venting the vacuum chamber.

Spectroscopic Measurements. Visible regime spectroscopic analyses were conducted using an ATR instrument described previously.[18] Modifications include the use of a spatial filter equipped with a 30 μm pinhole for a smaller probe beam diameter and a 1200 grooves/mm diffraction grating for improved spectral resolution. In the current work, coupling of the light beam into the IRE was performed in air with an internal angle of reflection (α) between 53° and 55° relative to the substrate normal. The spacing between the in-coupling and out-coupling prisms was 39.7 mm, yielding 14 to 15 reflections and a total illuminated area of approximately 0.36 cm^2. Probe beam propagation was along the long axis of the microscope slide (3 in. × 1 in.). Deposition of C_{13}-PTCDI films onto two orthogonally oriented substrates, as described above and in Fig. 1B, therefore allowed for measurements of $A_{TE,0°}$, $A_{TM,0°}$, $A_{TE,90°}$, and $A_{TM,90°}$.

Evanescent electric field intensity along each coordinate axis was calculated according to Harrick[28] for a three-phase layered structure using the following expressions:

$$E_x^2 = \frac{4\cos^2\alpha[\sin^2\alpha - (n_c/n_s)^2]}{[1 - (n_c/n_s)^2]\{[1 + (n_c/n_s)^2]\sin^2\alpha - (n_c/n_s)^2\}} \quad (11a)$$

$$E_y^2 = \frac{4\cos^2\alpha}{1 - (n_c/n_s)^2} \quad (11b)$$

$$E_z^2 = \left(\frac{n_c}{n_f}\right)^4 \frac{4\cos^2\alpha\sin^2\alpha}{[1 - (n_c/n_s)^2]\{[1 + (n_c/n_s)^2]\sin^2\alpha - (n_c/n_s)^2\}} \quad (11c)$$

where n_s, n_f, and n_c are the refractive indices of the internal reflection element (glass substrate), C_{13}-PTCDI film, and cladding or superstrate (air), respectively. The values used for n_s, n_f, and n_c were 1.51, 1.9,[29] and 1.00, respectively. The disilazane and PTFE layers were assumed to be too optically thin to significantly alter the properties of the evanescent field and were therefore ignored in these calculations.

Atomic Force Microscopy. The surface morphology of LB and vapor-deposited C_{13}-PTCDI films on silicon wafers or glass microscope slides, respectively, was examined using atomic force microscopy (AFM) performed in tapping mode on a Dimension 3100 Scanning Probe Microscope (Veeco Digital Instruments, Santa Barbara, CA). Rotated, oxide-sharpened silicon nitride tips were used in air, using contact-cantilevers in a tapping-mode configuration. To minimize distortion by contact forces between the tip and the sample, the minimum force required to obtain optimum resolution was used. The driving amplitude applied was the automated instrument default, between 100 and 400 mV. After the tip was engaged and imaging commenced, the setpoint value was increased until contact with the surface was lost and then incrementally decreased until optimal resolution was achieved. The samples were not altered by the AFM measurement, as noted by the invariance of successive AFM scans. The images presented below are representative of

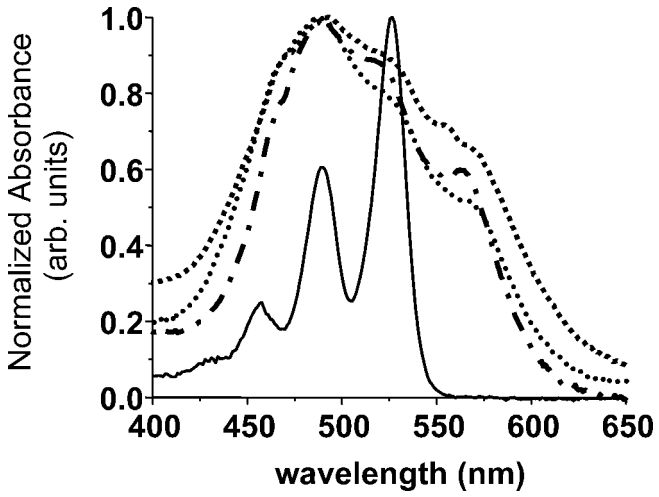

FIG. 3. The solution absorbance spectrum (×2.4) (——) of 2.6×10^{-6} M C_{13}-PTCDI dissolved in CH_2Cl_2 containing 10% (v/v) TFA is compared to ATR spectra of a LB monolayer acquired before (×1.8) (– – –) and after (×3.4) (·····) annealing, and a film of C_9-PTCDI that was vapor deposited onto oriented PTFE (×4.2) (–·–·–). Spectra are normalized by the factors stated above in parentheses for ease of comparison.

scans from different locations on the sample, different samples, and using different tips to image the surfaces.

RESULTS AND DISCUSSION

Alkyl disubstituted perylene diimides have been shown to irreversibly form a solid-phase Langmuir film due to strong intermolecular interactions and relatively weak interactions with the water subphase.[15] In particular, alkyl or alkoxy perylene derivatives exhibit strong π–π stacking interactions and side-chain interdigitation that produce a smectic liquid crystalline phase upon compression at the air–water interface[8] or evaporative deposition onto a variety of substrates.[13,14]

The pressure-area isotherm for C_{13}-PTCDI, shown in Fig. 2, is characterized by a single transition to a solid phase.[15] Further compression led to the formation of visible fibers oriented parallel to the trough barriers, indicative of heterogeneous multilayer formation and film collapse. The schematic diagram in Fig. 2 represents the proposed packing structure of C_{13}-PTCDI based on previous reports.[8,13,14]

A comparison of the dissolved and LB film absorbance spectra, plotted in Fig. 3, provides further evidence for the formation of an aggregated structure in the film. The solution phase spectrum contains four resolved bands with maxima at 432, 459, 489, and 527 nm, corresponding to the 0–3, 0–2, 0–1, and 0–0 transitions, respectively.[17,30] In contrast, ATR spectra of the LB films (shown in TE polarization) are considerably broadened and vibronic transitions are no longer resolved. For the unannealed LB film, a broad maximum is observed at 492 nm with shoulders at 471, 527, 555, and 567 nm, exhibiting an overall full-width at half-maximum (FWHM) of approximately 150 nm. Broadening and shifted transitions are attributed to exciton splitting in molecular assemblies that exhibit strong intermolecular forces, resulting in coupling of electronic transitions between parallel transition dipoles.[31] These spectral perturbations have been observed in numerous types of molecular assemblies, including LB[8] and evaporated films[13,14] of perylene-based materials.[17,30]

Annealing the LB film causes a narrowing of the spectroscopic FWHM to approximately 130 nm. The transitions are slightly shifted relative to the unannealed spectrum, occurring at 488, 525, and 570 nm, with a shoulder at 467 nm. The relative intensities (normalized to λ_{max}) of the peaks at 525 and 570 nm have dropped by approximately 10% as compared to the corresponding peaks in the unannealed spectrum. These differences clearly show that annealing alters the interactions between adjacent dyes in these thin films. The ATR spectrum of the vapor-deposited film is similar to that of the annealed LB film, although the absorbance bands are slightly better resolved, with peaks at 488 and 564 nm, and shoulders at 467 and 521 nm and an overall FWHM of 120 nm. The similarities in the spectra of the vapor-deposited and annealed LB films are not surprising since during vapor deposition, the substrate temperature was held at 100 °C, the same temperature at which LB films were annealed.

Example ATR spectra, at each substrate orientation and incident beam polarization, of LB and vapor deposited C_{13}-PTCDI films are shown in Fig. 4. A summary of the orientation parameters determined from these spectra is given in Table I. Note that the dichroic ratios r_{TE} and r_{TM} obtained for the LB films, both before and after annealing are not significantly different (i.e., $r_{TE} = r_{TM} = 1$, which leads to $\langle\mu_x^2\rangle = \langle\mu_y^2\rangle$) and the molecular orientation of the perylene core can be considered azimuthally uniaxial. Under these conditions, Eq. 8 becomes extremely sensitive to experimental errors as $\langle\mu_i^2\rangle/\mu^2$ approaches a limiting value resulting from division of zero over zero. However, for the uniaxial case, a treatment described by Bohn[32] and Saavedra,[33,34] in which it is assumed that $\langle\mu_x^2\rangle = \langle\mu_y^2\rangle$, can be utilized and the dichroic ratio is then defined as the ratio of the film absorbance in TE and TM polarizations by

$$\rho_{0^\circ} = \frac{A_{TE,0^\circ}}{A_{TM,0^\circ}}, \tag{12a}$$

$$\rho_{90^\circ} = \frac{A_{TE,90^\circ}}{A_{TM,90^\circ}} \tag{12b}$$

where the subscripts 0° and 90° refer to the two sample orientations. For an azimuthally isotropic film, $\rho_{0^\circ} = \rho_{90^\circ} = \rho$, and combining Eqs. 3–5 and 10 with Eq. 12 yields

$$\frac{\langle\mu_z^2\rangle}{\mu^2} = \frac{E_y^2 - \rho E_x^2}{2\rho E_z^2 + E_y^2 - \rho E_x^2} = \langle\cos^2\theta\rangle \quad \text{and} \tag{13}$$

$$\frac{\langle\mu_x^2\rangle}{\mu^2} = \frac{\langle\mu_y^2\rangle}{\mu^2} = \frac{\rho E_z^2}{2\rho E_z^2 + E_y^2 - \rho E_x^2} = \frac{1}{2}\langle\sin^2\theta\rangle \tag{14}$$

The normalized strengths of the transition dipole components along the three coordinate axes $\langle\mu_i^2\rangle/\mu^2$ were calculated using Eqs. 13 and 14 for the uniaxial case and are approximately equal for the unannealed film (Table I). The statistical equivalence of these values shows that the orientation distribution is completely isotropic with respect to all three coordinate axes. This can be described graphically by plotting an ellipsoid with semi-axes proportional to the dipole strength along each Cartesian di-

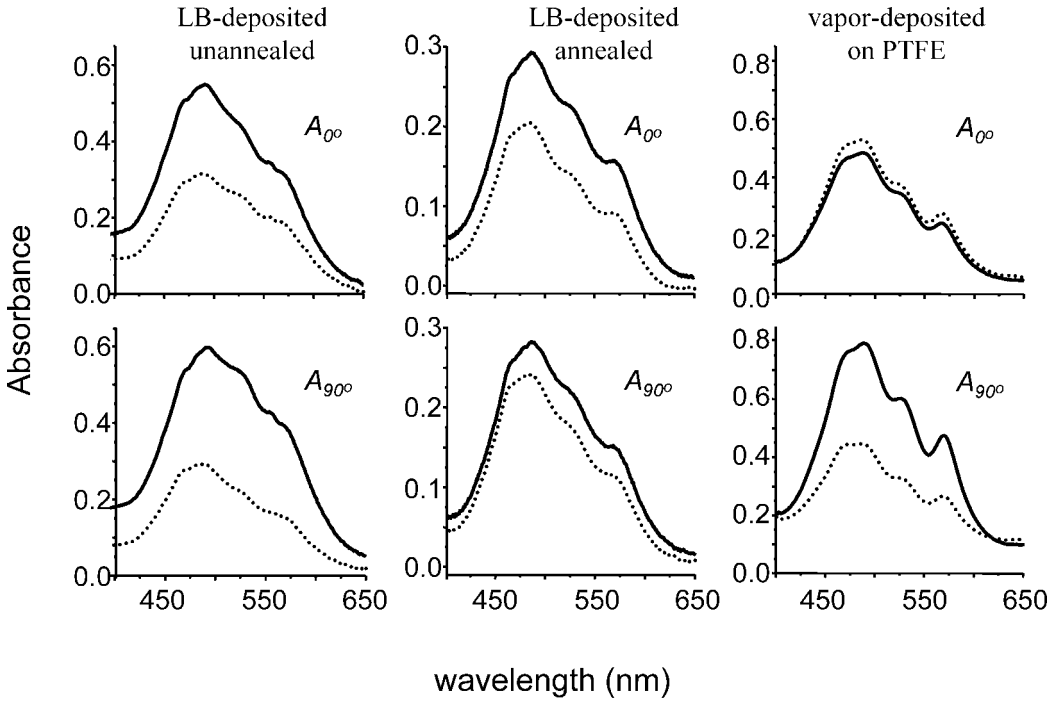

FIG. 4. Example ATR spectra of C_{13}-PTCDI films are shown for both sample orientations (0° and 90°) and at each incident beam polarization (TE (———) and TM (·····)).

rection; Fig. 5A depicts an approximately spherical distribution representing equal dipole intensity in all directions. Given the proposed packing structure shown in Fig. 2, these results suggest that while the π–π stacking of perylene cores results in microscopic ordering,[8,13,14] the aggregates form individual grains that, within the macroscopic scale of the measurement, are randomly oriented with respect to each other.

After annealing, r_{TE} and r_{TM} remain approximately equivalent ($r_{TE} = r_{TM} = 1$), while both $\rho_{0°}$ and $\rho_{90°}$ decrease significantly (Table I). This indicates that while the orientation distribution in the plane of the substrate (the *x–y* plane) remains isotropic, there is a significant increase in the dipole absorbance along the *z*-axis, orthogonal to the surface of the substrate. The out-of-plane absorbance dipole strength, $\langle\mu_z^2\rangle/\mu^2$ calculated with Eq. 13 (Table I), is significantly enhanced, graphically illustrated by the three-dimensional representation in Fig. 5B. Thus, annealing causes the molecules to align preferentially normal to the substrate.

TABLE I. Dichroic ratios and relative electronic transition dipole strengths for C_{13}-PTCDI films.

	LB unannealed	LB annealed	PTFE
r_{TE}	0.99 ± 0.07	0.94 ± 0.13	0.48 ± 0.08
r_{TM}	1.11 ± 0.07	1.0 ± 0.2	1.30 ± 0.12
$\rho_{0°}$	1.70 ± 0.06	1.2 ± 0.3	0.83 ± 0.05
$\rho_{90°}$	1.9 ± 0.2	1.3 ± 0.2	2.3 ± 0.4
$\langle\mu_x^2\rangle/\mu^2$	0.33 ± 0.03[a,c]	0.20 ± 0.03[a,c]	0.11 ± 0.03[d]
$\langle\mu_y^2\rangle/\mu^2$	0.33 ± 0.03[a,c]	0.20 ± 0.03[a,c]	0.05 ± 0.01[d]
$\langle\mu_z^2\rangle/\mu^2$	0.33 ± 0.06[a,b]	0.60 ± 0.05[a,b]	0.84 ± 0.05[d]

[a] Calculated using the average of $\rho_{0°}$ and $\rho_{90°}$.
[b] Calculated using the azimuthally uniaxial Eq. 13.
[c] Calculated using the azimuthally uniaxial Eq. 14.
[d] Calculated according to Eq. 8.

Morphological changes as a result of film annealing are illustrated by AFM images in Fig. 6A and 6B. In the height image of the unannealed LB film (Fig. 6A), aggregates of columnar structures are observed, with the column axes parallel to the plane of the substrate and a height of approximately 3 nm. Lateral interactions between columns are likely responsible for the formation of approximately parallel columns with lengths of up to 1 μm. However, examination of the entire 5 μm image reveals no evidence of long-range order in the substrate plane; thus, the in-plane molecular orientation of these aggregates appears to be random, consistent with the polarized spectroscopic results listed in Table I. Figure 6B shows that, after annealing, the columnar aggregates seen in Fig. 6A are replaced with amorphous, globular domains. As discussed above, enhanced out-of-plane molecular order, as measured by an increase in $\langle\mu_z^2\rangle/\mu^2$, accompanies this change in film morphology. However, the change in film morphology does not alter long-range order in the *x–y* plane, which remains isotropic.

Reflection infrared spectroscopy of vapor-deposited bis(*n*-propylimido)perylene has shown changes in molecular orientation as a result of thermal annealing in the presence of water vapor.[35] The angle between the plane of the perylene core and the plane of the substrate decreases upon annealing and is attributed to the intercalation of water through hydrogen bonding with the amido group. In the current study, the opposite effect was observed; the angle between the perylene core and the plane of the substrate increased after annealing.[35] This difference is likely due to the film preparation conditions. For films formed in vacuum, orientational changes were observed upon intercalation of water during annealing. For LB films originating from an aqueous subphase, the orientational change is likely due to exclusion of intercalat-

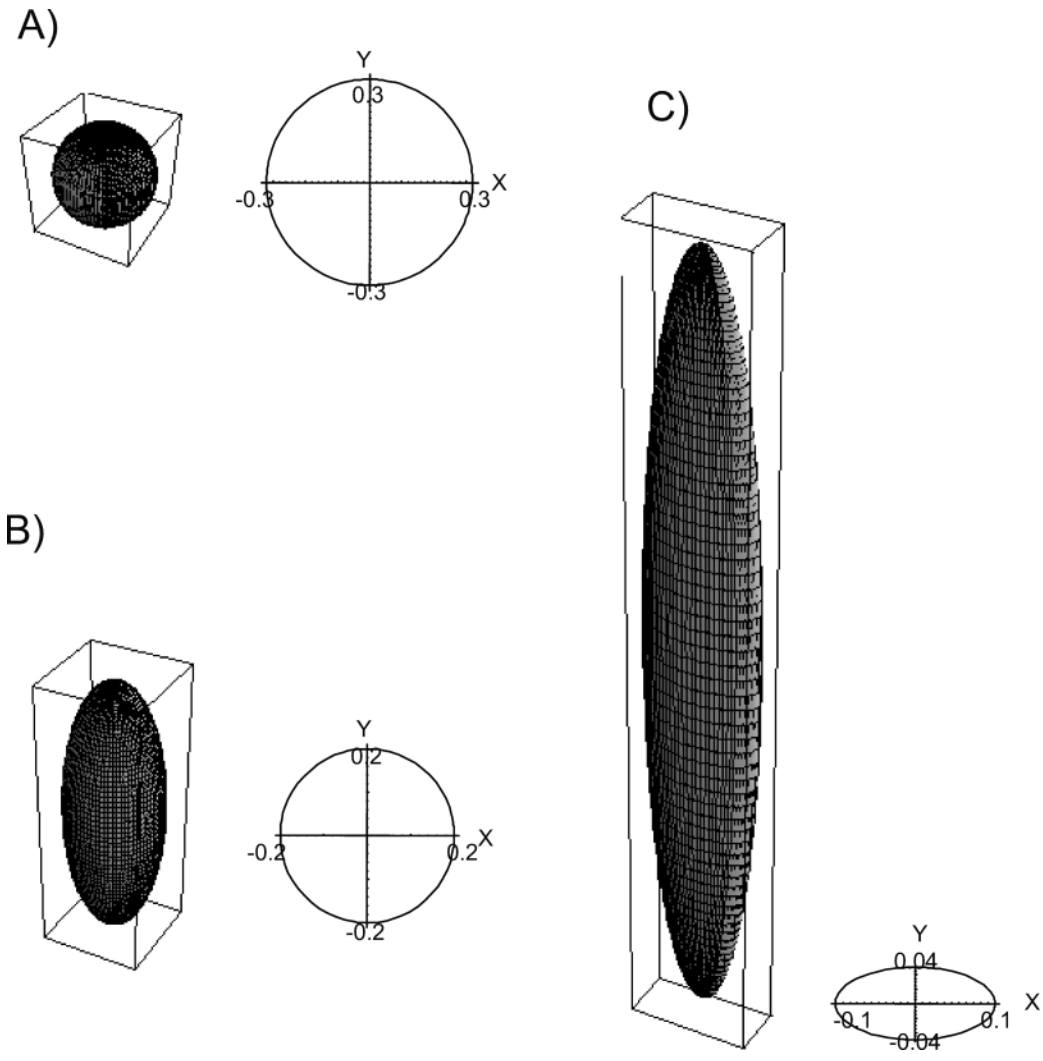

FIG. 5. The normalized intensities of the transition dipole components along the three coordinate axes are used to plot a three-dimensional figure (an ellipsoid) for LB films of C_{13}-PTCDI films (**A**) before and (**B**) after annealing, and (**C**) for a film vapor deposited onto an oriented PTFE substrate. To the right of each three-dimensional representation is a two-dimensional plot of the normalized dipole intensity in the plane of the substrate (the *x–y* plane defined in Fig. 1A).

ed water during annealing. Similar changes in molecular orientation, i.e., an increase of $\langle\mu_z^2\rangle/\mu^2$ following annealing, have been observed for LB films of liquid crystalline phthalocyanines deposited from an aqueous subphase.[19]

The vapor deposited films of C_{13}-PTCDI onto oriented PTFE show significant anisotropy for both in- and out-of-plane components (Table I). In the plane of the substrate, preferential absorption along the *x*-axis (the direction along which the PTFE block was pulled) is indicated by $r_{TE} < 1$ with a value of $\langle\mu_x^2\rangle/\mu^2$ that is twice that of $\langle\mu_y^2\rangle/\mu^2$ (Table I). This is illustrated graphically in Fig. 5C, which shows that the normalized transition dipole strength in the plane of the substrate is elliptical, with the *x*-axis corresponding to the long axis of the ellipse. However, the out-of-plane anisotropy is much greater. The large value of $\langle\mu_z^2\rangle/\mu^2$ shows that the perylene cores are oriented nearly perpendicular to the plane of the substrate. The three-dimensional orientational representation in Fig. 5C illustrates the differences in the relative transition dipole strength along all three axes.

Figure 6C shows the AFM image of the PTFE-modified substrate prior to vapor deposition of C_{13}-PTCDI. The horizontal stripes are the oriented PTFE columns, parallel to the substrate surface and aligned with the direction in which the PTFE block was pulled. The average height of the stripes is approximately 8 nm, with considerable variation, from 2 to 12 nm. Before PTFE deposition, the sessile water contact angle of the cleaned glass substrate was $<5°$. After deposition, it was 12°, which is much less than that expected for full coverage of PTFE ($>90°$),[36] indicating that glass substrate is exposed in the regions between the PTFE columns. The ellipsometric thickness of the PTFE film was 1.0 ± 0.5 nm, providing further evidence for relatively large areas of exposed glass.

After deposition of C_{13}-PTCDI, the columnar PTFE structures are still visible (Fig. 6D). The C_{13}-PTCDI film is evident as domain-like features located primarily between the columns of PTFE. The domains are approximately 3 nm high and are noticeably geometric in appearance, similar to those observed by Schlettwein et al.[14] for layered films of perylenetetracarboxylic anhydride (PTCDA) deposited on potassium bromide and chloride crystals. This morphology contrasts sharply with the

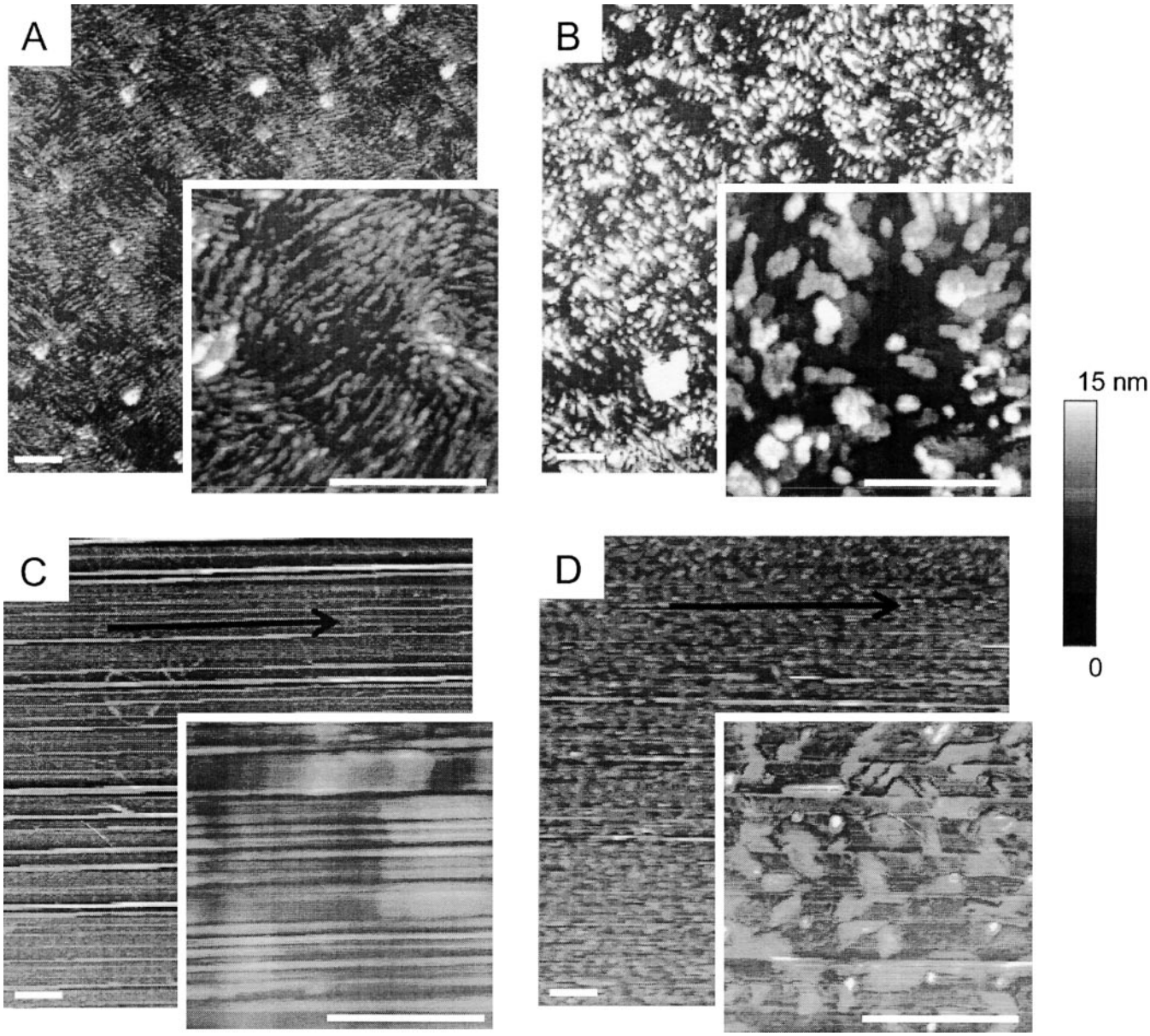

FIG. 6. AFM height images of films of C_{13}-PTCDI obtained using a scan area of 5 μm × 5 μm. The insets highlight a 1 μm^2 portion of each film. The scale bar in each image represents 500 nm. Images of LB films of C_{13}-PTCDI deposited on silanized (hydrophobized) Si wafers were acquired (**A**) before and (**B**) after annealing. The PTFE-modified glass substrate is shown (**C**) before and (**D**) after vapor deposition of C_{13}-PTCDI. The black arrows indicate the direction in which the PTFE block was pulled.

amorphous structures observed in the annealed LB films. Combined with the spectroscopic data showing in-plane orientational anisotropy with preferential orientation along the column direction, this suggests that the columns may serve as nucleation sites during film condensation, directing the orientation of the perylene core.

The existing literature contains considerable incongruity regarding the important factors dictating the molecular orientation of perylene adlayers. The orientational anisotropy of the films has been mainly attributed to π–π aggregation between neighboring molecules, while interactions between the substrate and the adsorbed film have been considered negligible.[8,15] In contrast, scanning tunneling microscopic (STM) studies of C_n-PTCDI derivatives deposited on MoS_2 and HOPG substrates demonstrated a preferential alignment of perylene domains with respect to the underlying substrate lattice.[14] In addition, the molecular orientation of surface-adsorbed perylene derivatives is influenced by varying degrees with appropriate choice of substituent,[37,38] application of mechanical shear force,[39,40] and by post-deposition annealing in the presence of water[35] or solvent[5] vapor. By making no *a priori* assumptions regarding substrate interactions or molecular structure, the current study emphasizes that both post-deposition processing, i.e., annealing, and choice of substrate can substantially affect the orientation of adsorbed perylene.

CONCLUSION

A visible-regime spectroscopic ATR method is described to elucidate molecular orientation of adlayer ma-

terials exhibiting a linear electronic transition dipole at monolayer coverages. The ensemble orientation is determined as the strength of the electronic transition dipole components in three dimensions, making no assumptions regarding the orientational distribution or substrate and intermolecular interactions. The technique was demonstrated using LB and vapor-deposited films of C_{13}-PTCDI on modified glass substrates.

Langmuir–Blodgett deposition of C_{13}-PTCDI monolayers onto silanized glass substrates yielded orientationally isotropic films of molecular aggregates. After annealing at 100 °C, the films displayed significantly enhanced absorption orthogonal to the plane of the substrate, indicating a preferential alignment of molecules normal to the substrate surface. However, the absorbance dipole strength in the plane of the substrate showed no macroscopic orientational preference: thus, annealing produces molecular aggregates with anisotropic out-of-plane orientation and isotropic in-plane orientation. In contrast, vapor deposition of C_{13}-PTCDI onto oriented PTFE-modified substrates yielded films with preferential electronic transition dipole alignment along the direction of the oriented PTFE film, and a large degree of out-of-plane orientation indicating dipole alignment nearly perpendicular to the plane of the substrate. These results demonstrate that both choice of substrate and post-deposition processing can influence the molecular orientation of perylene adlayers.

ACKNOWLEDGMENTS

This work was supported initially by the National Science Foundation under Grants Number CHE-0108805 (to S.S.S.) and CHE-0211900 (to N.R.A.), and in later stages by Grant Number DE-FG03-02ER15378 from Chemical Sciences, Geosciences and Biosciences Division, Office of Basic Energy Research, U.S. Department of Energy (to S.S.S. and N.R.A.). W.J.D. acknowledges fellowship support from a Proposition 301 Graduate Fellowship in Photonics. We thank Mr. Robert Davis (MONI) for AFM imaging and Dr. Hans Arwin (Laboratory of Applied Optics, IFM) for ellipsometric measurements.

1. A. M. van de Craats and J. M. Warman, Adv. Mater. **13,** 130 (2001).
2. V. Lemaur, D. A. Da Silva Filho, V. Coropceanu, M. Lehmann, Y. Geerts, J. Piris, M. G. Debije, A. M. Van de Craats, K. Senthilkumar, L. D. A. Siebbeles, J. M. Warman, J. L. Bredas, and J. Cornil, J. Am. Chem. Soc. **126,** 3271 (2004).
3. P. M. Kazmaier and R. Hoffmann, J. Am. Chem. Soc. **116,** 9684 (1994).
4. K. Y. Law, Chem. Rev. **93,** 449 (1993).
5. B. A. Gregg, J. Phys. Chem. **100,** 852 (1996).
6. B. A. Gregg and R. A. Cormier, J. Am. Chem. Soc. **123,** 7959 (2001).
7. B. A. Gregg, J. Phys. Chem. B **107,** 4688 (2003).
8. S. G. Liu, G. D. Sui, R. A. Cormier, R. M. Leblanc, and B. A. Gregg, J. Phys. Chem. B **106,** 1307 (2002).
9. G. Sui, J. Orbulescu, M. Mabrouki, M. Micic, R. M. Leblanc, S. G. Liu, R. A. Cormier, and B. A. Gregg, J. Phys. Chem. B **106,** 9335 (2002).
10. G. D. Sui, J. Orbulescu, M. Mabrouki, R. M. Leblanc, S. G. Liu, and B. A. Gregg, Chem. Phys. Chem. **3,** 1041 (2002).
11. C. L. Donley, W. Xia, B. A. Minch, R. A. P. Zangmeister, A. S. Drager, K. Nebesny, D. F. O'Brien, and N. R. Armstrong, Langmuir **19,** 6512 (2003).
12. C. L. Donley, R. A. P. Zangmeister, W. Xia, B. Minch, A. Drager, S. K. Cherian, L. LaRussa, B. Kippelen, B. Domercq, D. L. Mathine, D. F. O'Brien, and N. R. Armstrong, J. Mater. Res. **19,** 2087 (2004).
13. C. W. Struijk, A. B. Sieval, J. E. J. Dakhorst, M. van Dijk, P. Kimkes, R. B. M. Koehorst, H. Donker, T. J. Schaafsma, S. J. Picken, A. M. van de Craats, J. M. Warman, H. Zuilhof, and E. J. R. Sudholter, J. Am. Chem. Soc. **122,** 11057 (2000).
14. Y. Kaneda, M. E. Stawasz, D. L. Sampson, and B. A. Parkinson, Langmuir **17,** 6185 (2001).
15. R. Aroca, E. Johnson, and A. K. Maiti, Appl. Spectrosc. **49,** 466 (1995).
16. E. Johnson and R. Aroca, Appl. Spectrosc. **49,** 472 (1995).
17. P. A. Antunes, C. J. L. Constantino, R. F. Aroca, and J. Duff, Langmuir **17,** 2958 (2001).
18. W. J. Doherty, C. L. Donley, N. R. Armstrong, and S. S. Saavedra, Appl. Spectrosc. **56,** 920 (2002).
19. W. F. Flora, S. B. Mendes, W. J. Doherty, S. S. Saavedra, and N. R. Armstrong, Langmuir **21,** 360 (2005).
20. F. A. Hopf and G. I. Stegeman, *Applied Classical Electrodynamics* (John Wiley and Sons, New York, 1985).
21. J. Michl and E. W. Thulstrup, *Spectroscopy with Polarized Light* (VCH Publishers, New York, 1986).
22. E. E. Ross, L. J. Rozanski, T. Spratt, S. C. Liu, D. F. O'Brien, and S. S. Saavedra, Langmuir **19,** 1752 (2003).
23. P. E. Smolenyak, E. J. Osburn, S. Y. Chen, L. K. Chau, D. F. Obrien, and N. R. Armstrong, Langmuir **13,** 6568 (1997).
24. P. Smolenyak, R. Peterson, K. Nebesny, M. Torker, D. F. O'Brien, and N. R. Armstrong, J. Am. Chem. Soc. **121,** 8628 (1999).
25. D. A. Stephens and P. W. Bohn, Anal. Chem. **61,** 386 (1989).
26. J. C. Wittmann and P. Smith, Nature (London) **352,** 414 (1991).
27. D. Keyes, ''Optical Plastics,'' in *Handbook of Laser Science and Technology, Suppl. 2: Optical Materials* (CRC Press, Boca Raton, FL, 1995).
28. N. J. Harrick, *Internal Reflection Spectroscopy* (Harrick Scientific Corporation, Ossining, NY, 1979).
29. A. B. Djurisic, T. Fritz, and K. Leo, Opt. Commun. **166,** 35 (1999).
30. J. Mizuguchi and K. Tojo, J. Phys. Chem. B **106,** 767 (2002).
31. M. Kasha, H. R. Rawls, and M. A. El-Bayoumi, Pure Appl. Chem. **11,** 371 (1965).
32. D. M. Cropek and P. W. Bohn, J. Phys. Chem. **94,** 6452 (1990).
33. P. L. Edmiston, J. E. Lee, L. L. Wood, and S. S. Saavedra, J. Phys. Chem. **100,** 775 (1996).
34. J. E. Lee and S. S. Saavedra, ''Molecular orientation in adsorbed cytochrome c films by planar waveguide linear dichroism,'' in *ACS Symposium Series 602, Proteins at Interfaces II* (American Chemical Society, Washington, D.C., 1995).
35. A. P. Kam, R. Aroca, J. Duff, and C. P. Tripp, Langmuir **16,** 1185 (2000).
36. D. J. Wilson, R. L. Williams, and R. C. Pond, Surf. Interface Anal. **31,** 385 (2001).
37. M. Friedrich, G. Gavrila, C. Himcinschi, T. U. Kampen, A. Y. Kobitski, H. Mendez, G. Salvan, I. Cerrillo, J. Mendez, N. Nicoara, A. M. Baro, and D. R. T. Zahn, J. Phys.-Condens. Mat. **15,** S2699 (2003).
38. T. U. Kampen, G. Salvan, A. Paraian, C. Himcinschi, A. Y. Kobitski, M. Friedrich, and D. R. T. Zahn, Appl. Surf. Sci. **212,** 501 (2003).
39. T. D. Carson, W. Seo, S. W. Tam-Chang, and S. M. Casey, Chem. Mater. **15,** 2292 (2003).
40. I. K. Iverson, S. M. Casey, W. Seo, S. W. Tam-Chang, and B. A. Pindzola, Langmuir **18,** 3510 (2002).